Airborne Flux Measurements of BVOCs above Californian Oak Forests: Experimental Investigation of Surface and Entrainment Fluxes, OH Densities, and Damköhler Numbers

T. KARL,[*,+] P. K. MISZTAL,[#] H. H. JONSSON,[@] S. SHERTZ,[&] A. H. GOLDSTEIN,[#] AND A. B. GUENTHER[&]

[*] *Institute for Meteorology and Geophysics, University of Innsbruck, Innsbruck, Austria, and National Center for Atmospheric Research,** Boulder, Colorado*
[#] *University of California, Berkeley, Berkeley, California*
[@] *Center for Interdisciplinary Remotely-Piloted Aircraft Studies, Monterey, California*
[&] *National Center for Atmospheric Research,** Boulder, Colorado*

(Manuscript received 13 February 2013, in final form 7 May 2013)

ABSTRACT

Airborne flux measurements of isoprene were performed over the Californian oak belts surrounding the Central Valley. The authors demonstrate for the first time 1) the feasibility of airborne eddy covariance measurements of reactive biogenic volatile organic compounds; 2) the effect of chemistry on the vertical transport of reactive species, such as isoprene; and 3) the applicability of wavelet analysis to estimate regional fluxes of biogenic volatile organic compounds. These flux measurements demonstrate that instrumentation operating at slower response times (e.g., 1–5 s) can still be used to determine eddy covariance fluxes in the mixed layer above land, where typical length scales of 0.5–3 km were observed. Flux divergence of isoprene measured in the planetary boundary layer (PBL) is indicative of OH densities in the range of 4–7 $\times$ 10^6 molecules per cubic centimeter and allows extrapolation of airborne fluxes to the surface with Damköhler numbers (ratio between the mixing time scale and the chemical time scale) in the range of 0.3–0.9. Most of the isoprene is oxidized in the PBL with entrainment fluxes of about 10% compared to the corresponding surface fluxes. Entrainment velocities of 1–10 cm s^{-1} were measured. The authors present implications for parameterizing PBL schemes of reactive species in regional and global models.

1. Introduction

A number of direct flux measurements of conserved tracers (e.g., heat, water) have demonstrated their usefulness to investigate the horizontal and vertical structure of the atmosphere utilizing aircraft (e.g., Lenschow et al. 1980; Desjardins et al. 1997; Metzger et al. 2012). In contrast, only few direct flux measurements of reactive tracers exist to date. Faloona et al. (2005), for example, used a combination of ozone and dimethyl sulfide eddy covariance measurements to estimate accurate entrainment rates in the stable marine boundary layer. Mauder et al. (2007) investigated the influence of heterogeneous terrain on ozone deposition fluxes and the influence of mesoscale fluxes on the energy balance closure. Because of the lack of suitable flux measurements, most micrometeorological studies on reactive species in the mixed layer have been conducted with large-eddy simulations (LESs) (e.g., Schumann 1989; Peterson and Holtslag 1999; Patton et al. 2000; Vinuesa and Vila-Guerau de Arellano 2003). In the past, landscape-scale nonmethane volatile organic compounds (NMVOC) emissions were often estimated using mixed layer gradient techniques based on the results of LESs (e.g., Greenberg et al. 1999; Guenther et al. 1996). New advances in mass spectrometric methods have recently allowed investigation of urban anthropogenic NMVOC emissions based on direct airborne eddy covariance measurements (Karl et al. 2009). Such measurement systems provide a unique opportunity to constrain emissions of NMVOC that enter the atmosphere via biogenic and anthropogenic sources over regional spatial scales that are not directly

[+] Current affiliation: Institute for Meteorology and Geophysics, University of Innsbruck, Innsbruck, Austria.

** The National Center for Atmospheric Research is sponsored by the National Science Foundation.

Corresponding author address: Thomas Karl, Institute for Meteorology and Geophysics, University of Innsbruck, Innrain 52, 6020 Innsbruck, Austria.
E-mail: thomas.karl@uibk.ac.at

DOI: 10.1175/JAS-D-13-054.1

observable by any other known methods. The annual production of NMVOC (~1200–1350 TgC yr^{-1}) likely exceeds that of methane and CO (~500 TgC yr^{-1} each) (Goldstein and Galbally 2007). Emissions over land are thought to be responsible for more than 99% of the NMVOC in the atmosphere (Guenther et al. 1995) and biogenic volatile organic compound (BVOC) emissions dominate (Guenther et al. 2006). Here we expand airborne flux measurements of BVOC to investigate the atmospheric fate of reactive compounds above forested areas, which are thought to the dominant global source of BVOC. The California Airborne BVOC Emission Research in Natural Ecosystem Transects (CABERNET) experiment took place over extended oak belts surrounding the Central Valley (34°32′–39°21′N, 117°28′–123°17′W) during June 2011. The study focused on isoprene (2-methyl–1,3–butadiene), a biogenic hydrocarbon, which is thought to be emitted to the atmosphere in similar amounts on a mass basis compared to methane (Guenther et al. 2006). Isoprene fluxes were measured on board the Center for Interdisciplinary Remotely-Piloted Aircraft Studies (CIRPAS) Twin Otter (http://www.cirpas.org/twinOtter.html) using the virtual disjunct eddy covariance method (Karl et al. 2002). Here we focus on three out of eight research flights aimed at extensive vertical profiling in and above the planetary boundary layer. This article presents the first direct airborne isoprene flux measurements focused on vertical flux profiles; fluxes of isoprene and other BVOC from survey transects and their comparison to modeled fluxes are presented in a separate paper (Misztal et al. 2013, unpublished manuscript). We demonstrate how these measurements can be used to constrain surface and entrainment fluxes as well as reactive losses due to reaction with the OH radical and so enabling area-averaged estimates of OH. In particular, we demonstrate the usefulness of short-lived (i.e., $\tau < 1$ h) tracers to investigate entrainment fluxes.

2. Experimental method

a. CIRPAS Twin Otter

The CIRPAS Twin Otter is a twin-engine turboprop aircraft operated by the Naval Postgraduate School in Monterey, California. It is equipped with state-of-the-art sensors for meteorological research missions. The CIRPAS payload during CABERNET included total temperature measured by a rosemount probe, dewpoint temperature (chilled mirror, EdgeTech Inc., United States); barometric, dynamic, and radome-angle pressures based on barometric and differential transducers (Setra Inc., United States); true air speed (TAS), mean wind, and slip and attack angles measured by a radome flow-angle probe; GPS pitch, roll, and heading [Trimble Advanced Navigation System (TANS) Vector platform attitude, Trimble Inc., United States]; GPS latitude, longitude, altitude, ground speed, and track (NovAtel, Inc., United States); and latitude, longitude, altitude, ground speed, and track, pitch, roll, and heading measured by Coarse/Acquisition (C/A)-code Miniature Integrated GPS/ Inertial Navigation System (INS) Tactical System III (C-MIGITS-III) (GPS/INS, Systron, Inc., Canada).

The sampling setup for in situ instrumentation was based on an isokinetic pipe flushed with ram pressure. The VOC inlet duct (ID) was 3 in. (1 in. = 2.54 cm), diffused from a 2.047-in. ID orifice at the tip (area ratio of about 2). The tip is inside another diffuser with an area ratio of 5, resulting in a flow speed inside the tube of about 1/10 of the aircraft speed (6–7 m s^{-1}). The mission aircraft speed was between 60 and 70 m s^{-1}.

b. National Center for Atmospheric Research (NCAR) PTR-MS

A redesigned proton-transfer-reaction mass spectrometer (PTR-MS) based on Karl et al. (2009) was deployed to measure VOC fluxes by the virtual disjunct eddy covariance technique (Karl et al. 2002). A detailed description about operating conditions and instrument validation was previously documented (de Gouw et al. 2003). The instrument was typically operated at 2.3-mb drift pressure and 560-V drift voltage. Isoprene was calibrated using a multicomponent NMVOC standard, which contained a mixture of methanol, acetonitrile, acetaldehyde, acetone, isoprene, methyl vinyl ketone, methyl ethyl ketone, benzene, toluene, m-, o-, p-xylenes, and camphene. Typical instrument sensitivities for isoprene were 15 normalized counts per second per part per billion by volume [ncps $(ppbv)^{-1}$], where count rates are normalized by a standard primary ion count rate of 1×10^6 counts per second (cps), which for a primary ion signal of about 2×10^7 cps led to a sensitivity of 300 cps $(ppbv)^{-1}$. The disjunct sampling interval was 0.5 s at 5-Hz sampling frequency. Lenschow and Kristensen (1985) reviewed instrumental requirements to accurately measure fluxes F in the mixed layer. The required instrument sensitivity for uncorrelated noise to be negligible is $S = Q/(\langle c\rangle \Gamma/dt)$, where $\langle c\rangle$ is the concentration, dt the sample interval, and Γ is the integral time scale. The total counts required Q must be greater than $\langle c\rangle^2/(4\sigma_c^2)$; thus, one can derive a critical threshold for the mixed layer, where

$$Q > 0.15 \frac{w_*^2 \langle c\rangle^2}{F^2}. \quad (1)$$

During CABERNET $F/\langle c\rangle$ ratios for isoprene were in the range from 0.09 to 0.4 m s^{-1}. Typical length scales

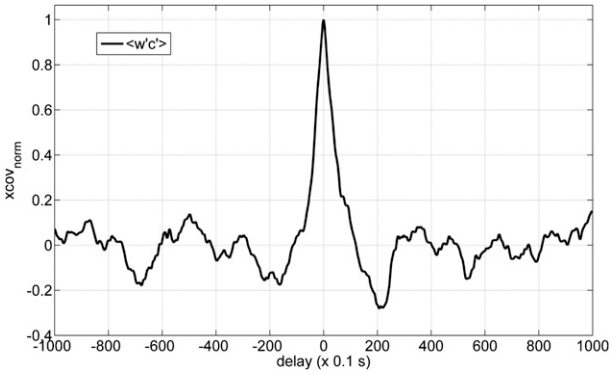

FIG. 1. Normalized covariance between w' and c' measured during RF3.

in the mixed layer are 100 m, leading to Γ of 100 m/60 m s^{-1} = 1.6 s for this study. For w^* = 2 m s^{-1} and typical isoprene concentrations of 1 ppbv we calculate required count rates of 2.3–46 counts within one integral time scale. The integrated count rate over Γ during this study was 300 × 0.2/0.5 × 1.6 = 192 counts—thus sufficient for measuring isoprene fluxes. Figure 1 shows a typical example of the covariance between isoprene and vertical wind velocity measured at 300 m AGL.

The delay time through the isokinetic pipe was estimated to be less than 0.2 s. The PTR-MS was connected to this flow via a 3-m-long 1/4-in. Teflon [perfluoroalkoxy (PFA)] line (ID = 0.5 cm) pumped by a sampling pump at a flow rate of about 1.5 L min^{-1}. This led to an overall delay time of about 2.4 s.

c. *Research flight pattern*

The vertical profiling strategy was developed to optimize aircraft speed and maneuverability with sufficient horizontal-averaging statistics. Figure 2 depicts a map showing the CABERNET study area. Research flights 3, 6, and 7 (RF3, RF6, and RF7, respectively) were planned so that profiles could be flown between 1200 and 1600 local time. RF3 targeted an area northwest of Sacramento between waypoints 39°04′53″N, 121°09′32″W and 39°13′50″N, 121°07′12″W. RF6 and RF7 were conducted east of Madera between waypoints 37°02′31″N, 119°44′95″W and 37°14′10″N, 119°50′05″W. The profiles were flown at 1010–1240, 1035–1500, and 1240–1500 Pacific standard time (PST) during RF3, RF6, and RF7, respectively. On the incoming leg, a saw-tooth sounding was performed in order to determine the height of the planetary boundary layer (PBL) at the start of the

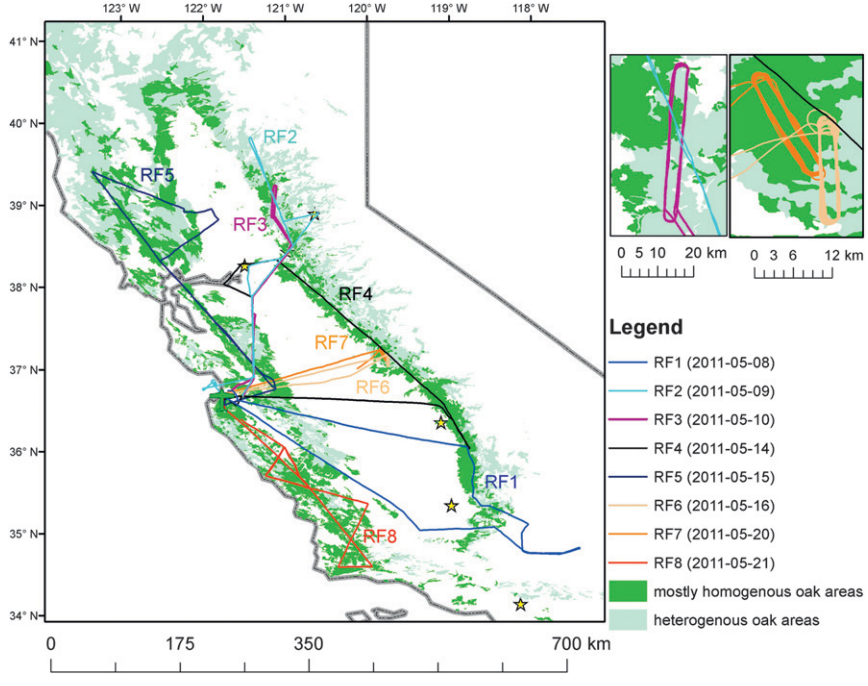

FIG. 2. Map showing the area covered by CABERNET research flights. Race-track patterns flown during RF3, RF6, and RF7 are highlighted in separate panels. These flight tracks are plotted on a map that shows two habitats from the Gap Analysis Program (GAP) land cover database used by the California Air Resources Board (CARB). The primary (i.e., homogeneous) oak habitats comprised blue, coastal, and valley oak woodlands. Heterogeneous oak areas were using three other habitats from the GAP database, which included foothill pine, montane hardwood, and conifer woodlands that contain oaks as secondary habitats.

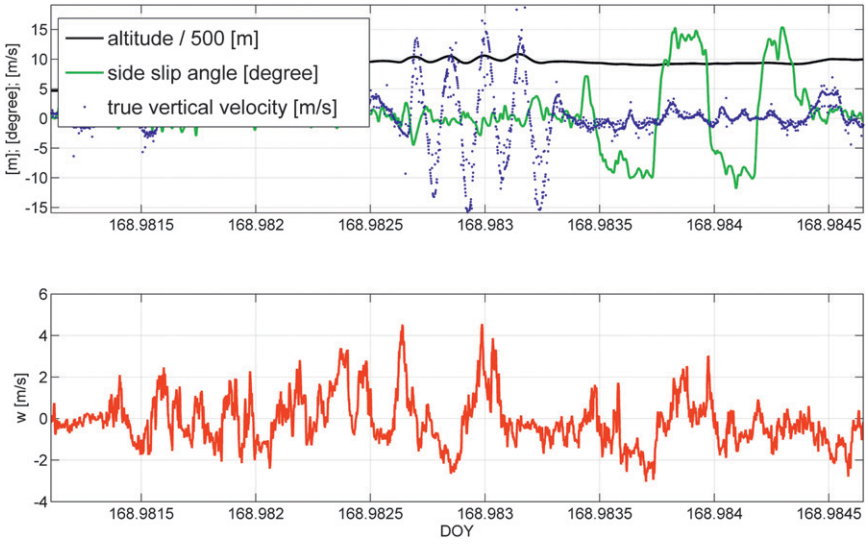

FIG. 3. Side-slip-and-pitch maneuver during RF6: the x axis presents day of the year (DOY). (top) Side-slip-angle (green), altitude (black), and true vertical velocity (blue) (calculated as dz/dt); (bottom) motion-corrected vertical wind speed.

profiling maneuver. A stacked profile consisting of 3 (RF3) or 5 (RF6 and RF7) levels was then spaced equally between 300 m AGL and the height of the PBL. A racetrack of 40 km (RF3) or 16-km length (RF6 and RF7) and 2-km width was flown at each level descending from the top. After two profiles (down and up) another sounding in the form of a spiral was conducted. Thus, one profile was completed in about 45 min during RF6 and RF7 and in 70 min during RF3. Following the last profile another saw-tooth sounding was flown on the outbound leg. The shorter length during RF6 and RF7 was a final compromise between constraints imposed by footprint, stationarity, and available operational time on the aircraft. The PBL height typically varied by less than 15% during RF3, RF6, and RF7 profiling maneuvers.

After each research flight, in-flight calibrations of the radome pressure system were performed by conducting a side-slip-and-pitch maneuver (e.g., Lenschow et al. 1978). Reverse heading and speed maneuvers were conducted during the test flight. Figure 3 shows corrected vertical wind velocity during a side-slip (indicated by side-slip angle)-and-pitch (indicated by altitude) maneuver and true vertical velocity of the plane. The vertical aircraft motion (sinusoidal altitude variation) during the pitch maneuver was $\pm 15\,\mathrm{m\,s^{-1}}$, significantly larger than any vertical motion during flux legs (e.g., ± 1–$3\,\mathrm{m\,s^{-1}}$). The plot suggests that the correction procedure works reasonably well for flux legs, where the side-slip angle was typically less than 3° and the pitch less than $\pm 3\,\mathrm{m\,s^{-1}}$. Systematic (SE) and random errors (RE) for eddy covariance measurements on aircraft have been discussed by Lenschow et al. (1994):

$$\text{systematic error} \le \frac{2.2 z_i (z/z_i)^{1/2}}{L} \quad \text{and} \tag{2}$$

$$\text{random error} \le 1.75 \times \left(\frac{z}{z_i}\right)^{1/4} \left(\frac{z_i}{L}\right)^{1/2}, \tag{3}$$

where z_i is the planetary boundary layer height, z is the flight altitude, and L is the length of the flight leg. Here we average across the entire length of the straight portions of the racetracks (excluding turns). For conditions during RF6 and RF7 we calculate an SE of 3% at the lowest flight level, increasing to about 10% at the highest flight level. The RE varied between 15% at the lowest level and 26% at the highest level. For RF3 these errors were calculated in the range of 1%–4% for the SE and 10%–17% for the RE.

Generally, slow aircraft speeds can reduce the bias due to disjunct sampling strategies. Following Lenschow et al. (1994), we calculate the relative systematic error of fluxes measured by the virtual disjunct eddy covariance method. The integral time scale obtained from Fig. 1 is 1.66 s, which at an air speed of $60\,\mathrm{m\,s^{-1}}$, comes close to a length scale of 100 m. The virtual disjunct sampling interval Δ divided by Γ was therefore 0.3. The error due to virtual disjunct sampling, where the averaging interval T is much larger than Γ, can therefore be calculated in its asymptotic form, where $\Delta < \Gamma$:

$$\frac{F - F_{\text{disjunct}}}{F} = 2\frac{\Gamma}{T}. \quad (4)$$

Equation (4) leads to a systematic error of 6‰ for RF6 and RF7 and 2.5‰ for RF3. We conclude that a virtual disjunct sampling interval of 0.5 s was sufficiently small to have a negligible effect on the calculated fluxes. The combined systematic error is given by the sum of Eqs. (2) and (4) and thus dominated by the systematic error due to the imposed horizontal averaging length.

The random error variance of the flux due to virtual disjunct sampling can be calculated according to

$$\frac{\sigma^2_{\text{disjunct}}}{\sigma^2} = \frac{\Delta}{2\Gamma}\coth\left(\frac{\Delta}{2\Gamma}\right), \quad (5)$$

where σ_{disjunct} represents the standard deviation of the disjunct eddy covariance (DEC) flux compared to a continuously measured flux σ (Lenschow et al. 1994). For $\Delta = 0.5$ s and $\Gamma = 1.7$ s we calculate the relative random error variance of the flux due to virtual disjunct sampling to be 1.007. This would increase to 1.02 for $\Gamma = 1.0$ s. Thus, the relative error due to virtual disjunct sampling would increase the error variance of the flux by about 7‰–2%. The combined upper limit of the random error in the lower part of the mixed layer [Eqs. (3) and (5)] is therefore dominated by Eq. (3).

3. Flux method and theory

a. Theoretical considerations

The budget equation of a scalar is

$$\frac{\partial C}{\partial t} + \mathbf{u}\frac{\partial C}{\partial \mathbf{x}} = S, \quad (6)$$

where C is the concentration, which can generally be decomposed into a mean and fluctuating part ($C := \langle c\rangle + c'$), $\mathbf{u}$ ($:=u, v, w$) is the three-dimensional wind vector corresponding to the coordinates $\mathbf{x}$ ($:=x, y, z$), and S is the local net source or sink term.

Typical subsidence rates are on the order of 1 cm s^{-1} and small compared to convective velocity scales w^* of 1–2 m s^{-1} observed during CABERNET. We therefore ignore the mean vertical motion $\langle w\rangle$. After decomposition of $\mathbf{u}$ into mean and turbulent parts, and assuming negligible horizontal turbulent parts, we arrive at

$$\frac{\partial\langle c\rangle}{\partial t} + \langle \mathbf{u}_{x,y}\rangle\frac{\partial\langle c\rangle}{\partial \mathbf{x}_{x,y}} + \frac{\partial\langle w'c'\rangle}{\partial z} = S, \quad (7)$$

where the second term on the left-hand side represents horizontal advection and the third term on the left-hand side is the vertical flux divergence. Since the horizontal advection term is typically an order of magnitude larger than turbulent terms, the horizontal turbulent term is dropped in Eq. (7).

The loss term (S) for isoprene can be approximated by a simple first-order loss rate, where the lifetime τ equals $1/(k_{\text{OH}}[\text{OH}] + k_{\text{O3}}[\text{O}_3] + k_{\text{NO3}}[\text{NO}_3])$ and k_{OH}, k_{O3}, and k_{NO3} represent reaction rates with respect to OH, O_3, and NO_3; typical ozone concentrations during CABERNET profiles were measured in the range of 50–80 ppbv leading to an isoprene lifetime of 11–17 h owing to reaction with ozone. The NO_3 radical is thought to play a minor role during daytime. The midday lifetime of NO_3 due to photolysis [$\tau(h\nu)$] is about 4.8 s. Neglecting other loss reactions (e.g., $NO_3 + NO_2 \leftrightarrow N_2O_5$), the lower limit for the isoprene lifetime with respect to reaction with NO_3 is about 3 days (50 ppbv O_3, 1 ppbv NO_x). Based on a steady state calculation (e.g., Kim et al. 2013), where O_3 = 50–80 ppbv, NO_2 = 0.1–1 ppbv (e.g., Shilling et al. 2013), HO_2 = 60 pptv, H_2O = 1%, and OH reactivity = 3–15 s^{-1}, typical noontime OH concentrations would lie between 78 ppq amd1.4 pptv; we therefore assume that the lifetime of isoprene (5 min–1.4 h) is mainly controlled via the OH radical during daytime.

b. Flux analysis

We deploy conventional fast Fourier transform (FFT) and wavelet analysis to investigate turbulent fluxes. Briefly, following general considerations outlined by Torrence and Compo (1998) and considering bias rectification proposed by Liu et al. (2007), we implemented a wavelet transformation routine using the Morlet wavelet (Thomas and Foken 2005). Two advantages of wavelet transforms include that 1) it does not rely on the ergodic hypothesis and therefore does not require stationarity and 2) it allows investigating time-resolved spectral contributions to the measured flux. Figure 4 shows a typical example of a normalized power spectrum for sensible heat and isoprene flux using conventional FFT and wavelet transformation. It should be noted that the spectral analysis of VOC data is limited to the Nyquist frequency imposed by the disjunct sampling interval of 0.5 s. Integrated cospectra (i.e., fluxes) typically agreed to within ±10% between FFT and wavelet transforms for the profiling flights. The rationale for using wavelet analysis is that a substantial part of the CABERNET mission was dedicated to the investigation of horizontally segregated patterns of isoprene surface fluxes, which will be published in a second manuscript (Misztal et al. 2013, unpublished manuscript).

The advection flux was calculated parallel and perpendicular to each racetrack. For RF03, RF06, and RF07 the advection fluxes were on the order of 28%, 4.9%, and

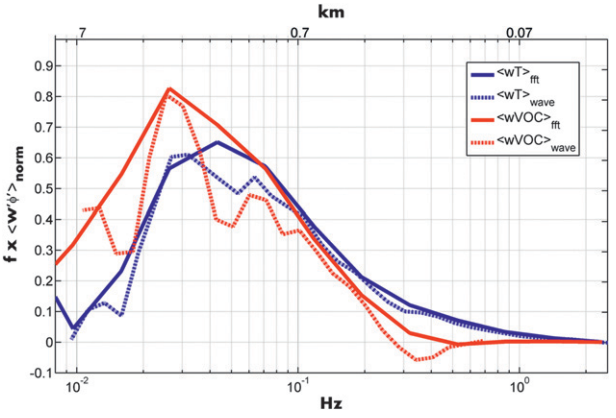

FIG. 4. Normalized cospectra of isoprene (red) and temperature (blue) with vertical wind. Dashed lines indicate spectra calculated by wavelet transformation; solid lines are obtained by conventional FFT. The top axis indicates the spatial scale corresponding to an aircraft speed of 70 m s^{-1}.

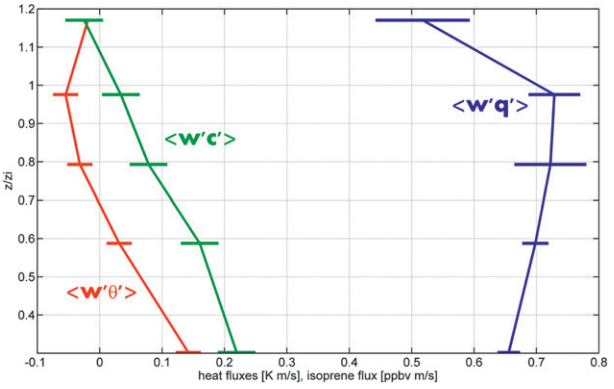

FIG. 5. Kinematic heat (red: $\langle w'\theta'\rangle$, blue: $\langle w'q'\rangle$) and isoprene (green: $\langle w'c'\rangle$) fluxes for RF6. Error bars (1σ) indicate the variability of all flux profiles flown during RF6.

3.8% relative to the average turbulent flux of isoprene. Because of a limited vertical resolution of three levels in total and only two obtained in the PBL at $z/z_i = 0.7$ and $z/z_i = 0.95$, further analysis of concentration gradients will therefore mainly focus on RF6 and RF7.

Sufficiently strong northwesterly winds during RF6 and RF7 prohibited the establishment of the Fresno eddy (e.g., Lin and Jao 1995), leading to consistent upslope winds during these research flights. Profiles were flown during cloudless conditions. The footprint was calculated according to parameterizations for the convective mixed layer according to Weil and Horst (1992):

$$dx_{0.5} = 0.9\frac{uz_m^{2/3}h^{1/3}}{w*}, \tag{8}$$

where $dx_{0.5}$ is the half-width of the horizontal footprint, u is the horizontal wind speed, z_m is the height above ground, and h is the PBL height. The half-width is defined as the horizontal distance between points where the flux footprint falls to one-half of its maximum value. Equation (8) can be regarded as a horizontal footprint scale. As an example, this leads to a typical half-width of the horizontal footprint of 3.1 km for $h = 2000$ m, $z_m = 1500$ m, $u = 3.5$ m s^{-1}, and $w* = 1.7$ m s^{-1} encountered during RF6. The fetch (i.e., the spatial extent of the oak forest upwind) was about 12 km for RF6 and RF7.

4. Flux profiles

a. Heat and isoprene fluxes

Figure 5 depicts the average of all measured kinematic heat fluxes ($\langle w'\theta'\rangle$ and $\langle q'w'\rangle$) as well as isoprene fluxes for RF6. We generally define the height of the PBL as minimum of the $\langle w'\theta'\rangle$ at the inversion. $\langle w'q'\rangle$ generally decreased at the inversion layer. The $\langle w'q'\rangle$ profile suggests a relatively wet PBL when compared to the free troposphere (FT), and follows a very similar flux profile compared to idealized LES runs (e.g., Patton et al. 2005).

Reducing the buoyancy flux equation to

$$\frac{\partial\langle\theta\rangle}{\partial t} = -\frac{\partial\langle w'\theta'\rangle}{\partial z}, \tag{9}$$

we can test whether the flux divergence of the buoyancy flux is comparable to the heating rate of the PBL by assuming a linear flux profile ($\langle w'\theta'\rangle = a - bz$). This leads to a simple expression where the heating rate is equal to the linearized PBL slope of $\langle w'\theta'\rangle$ in Fig. 5. From Fig. 5 we obtain $b = 0.6 \pm 0.1$ K h^{-1}. The observed temperature change $\partial\langle\Theta\rangle/\partial t$ was 0.4 ± 0.2 K h^{-1}. Isoprene fluxes linearly decrease throughout the PBL owing to its short atmospheric lifetime. From the slope we can calculate the lifetime, OH density, and Damköhler number (Da), which is defined as the ratio of the mixing time scale to the chemical time scale. Table 1 summarizes these quantities for RF3, RF6, and RF7. Entrainment velocities ($v_e := F_e/\Delta C$) are obtained by extrapolating the isoprene flux profile to the top of the PBL and taking the concentration jump between the PBL and FT, where PBL concentrations are extrapolated to the entrainment zone. Calculated entrainment velocities are 5.5, 9.6, and 1.4 cm s^{-1} for RF3, RF6, and RF7, respectively. Estimating entrainment velocities from isoprene or other scalars that can roughly be approximated by a similarly fast first-order decay has the advantage that these species exhibit a significant concentration jump across the entrainment zone. For example, isoprene concentrations above the ML were less than 0.1 times the ML concentration. This allows for accurately constraining the concentration

TABLE 1. Summary of PBL height, w^*, τ, OH density, Damköhler number, isoprene fluxes, and entrainment velocity for RF3, RF6, and RF7.

	PBL height (m)	w^* (m s^{-1})	τ (s)	OH (molecules per cubic centimeter)	Da	$F(z/z_i)$ (ppbv m s^{-1})	v_e (cm s^{-1})
RF3	1000 ± 100	2.0 ± 0.3	2300 ± 50	(4.4 ± 0.3) × 10^6	0.2	−(0.32 ± 0.08) × z/z_i + (0.33 ± 0.08)	5.5 ± 1.0
RF6	2000 ± 100	1.7 ± 0.3	1520 ± 50	(6.6 ± 0.3) × 10^6	0.9	−(0.31 ± 0.05) × z/z_i + (0.28 ± 0.05)	9.6 ± 1.5
RF7	1200 ± 100	2.0 ± 0.3	1400 ± 50	(7.2 ± 0.3) × 10^6	0.5	−(0.21 ± 0.03) × z/z_i + (0.22 ± 0.03)	1.4 ± 0.3

jump ΔC across the entrainment zone owing to small free-tropospheric concentrations.

In situ OH observations still remain challenging (Mauldin et al. 2012; Williams et al. 2011) and recent debate about the magnitude of the oxidizing capacity of the atmosphere in isoprene dominated environments has fueled speculation about unknown OH recycling mechanisms (Lelieveld et al. 2008; Hofzumahaus et al. 2009). Vilà-Guerau de Arellano et al. (2011) performed a sensitivity analysis illustrating the interrelationship between physical and chemical constraints on OH loss and production rates in the PBL; they suggest that vertical transport terms need to be considered when interpreting field datasets of isoprene concentrations. Our measurements demonstrate that the isoprene flux divergence follows a linear dependency, as has been suggested previously by LES modeling studies (e.g., Vinuesa and Vila-Guerau de Arellano 2003). In addition, we show that isoprene flux divergence measurements can be successfully used to assess the average oxidizing power of the PBL without any assumptions. Based on flux divergence measurements we determine OH densities in the range of 4–7 × 10^6 molecules per cubic centimeter. The lifetime was calculated from the slope dF/dz, divided by the mean ML concentration. OH densities were based on the rate constant between the {OH + isoprene} reaction (k_{iso} = 2.5 × 10^{-11} × $e^{410/T}$). Damköhler numbers up to 0.9 suggest that the chemical reactivity of isoprene is comparable to its turnaround time in the PBL. We further investigate the influence on the modified diffusion coefficient for a first-order PBL parameterization scheme.

b. *Comparison between measurements and PBL scheme*

Figure 6 compares measured $d\theta_v/dz$ profiles with a calculated profile based on one commonly used PBL scheme [Yonsei University (YSU); Hong et al. 2006]. The YSU scheme is based on earlier first order nonlocal diffusion schemes (e.g., Troen and Mahrt 1986), which have been extensively used in mesoscale and global models. Overall the model is in reasonably good agreement with CABERNET measurements.

We normalize data shown in Fig. 6 by defining a local diffusion coefficient according to

$$K := -\frac{\langle w'\theta_v' \rangle}{\partial \theta_v / \partial z}. \tag{10}$$

Figure 7 depicts K plotted as a function of PBL height for RF6 and RF7.

For a reactive species, such as isoprene, the diffusion coefficient has to be modified. The advantage of the present experimental dataset is that we measure both flux and concentration gradients that allow investigating the simplest parameterization of a chemistry–turbulence modification term. Following Kristensen et al. (1997) and Hamba (1993) we adopt the following expression for a first-order loss:

$$K_{\text{reactive}} = \frac{K}{1 + \text{Da}}. \tag{11}$$

Figure 8 illustrates the effect of chemically reactive species, which leads to a decrease of the local diffusion coefficient. The local diffusion coefficient based on flux observations is smaller for isoprene than for a conserved tracer. Correction according to Eq. (11) reduces the discrepancy between measured and modeled diffusion coefficients. It is noted that this effect would not be accounted for by a separate chemical operator in a coupled model, as long as the model does not explicitly calculate vertical transport in the PBL. The modified local diffusion coefficient will alter the concentration gradient and

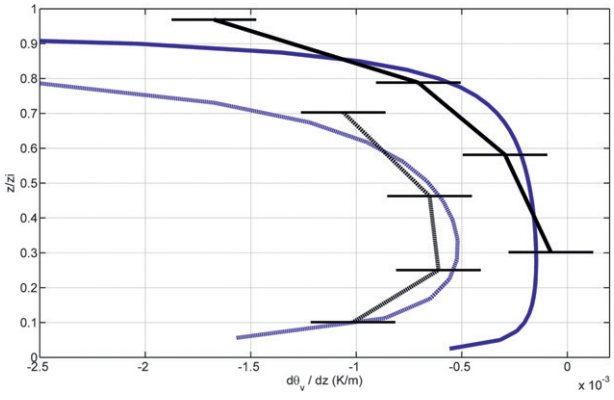

FIG. 6. Measured (black) and simulated (blue) $d\theta_v/dz$ profiles. The solid lines represent RF6 and the dashed lines RF7.

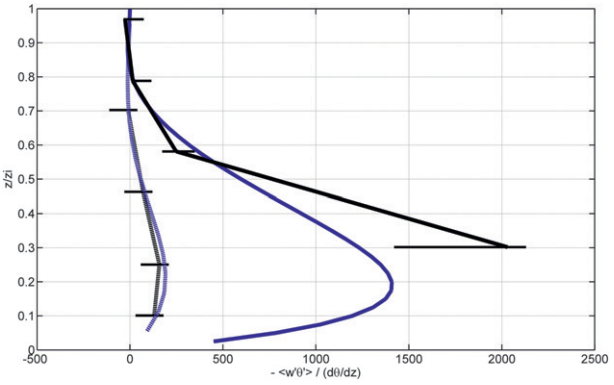

FIG. 7. Local diffusion coefficient plotted vs z/z_i. Black lines represent measured diffusion coefficients for RF6 (solid) and RF7 (dashed); blue lines are the corresponding modeled diffusion coefficients.

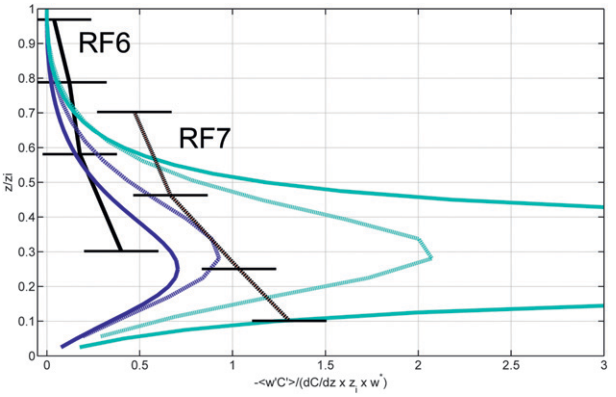

FIG. 8. Normalized diffusion coefficient for isoprene for RF6 (solid) and RF7 (dashed). Black lines represent measurements. Bars indicate 1σ. The cyan lines are the modeled diffusion coefficient for a nonreactive species for RF6 and RF7, respectively. The blue lines depict the modeled diffusion coefficients corrected by the Damköhler number.

consequently also impact the modeled flux divergence. A first-order loss modification according to Eq. (11) would bring modeled and measured concentrations more in line with a second-order closure model, which provides a prognostic equation for the evolution of second-order moments (i.e., flux) as suggested by Hamba (1993). Kristensen et al. (1997) postulated that, in the surface layer, the error of an estimated flux based on a noncorrected diffusion coefficient should be equal to the Damköhler ratio. In analogy we discuss the impact on bottom-up–top-down diffusion functions (e.g., Moeng and Sullivan 1994; Patton et al. 2003) that have been used for the mixed-layer gradient (MLG) method to obtain fluxes (Greenberg et al. 1999; Spirig et al. 2004; Karl et al. 2007). Fluxes estimated based on the MLG method rely on inverting mixed-layer concentration measurements by splitting the contribution into a bottom-up (BU) and top-down (TD) diffusion process. Parameterization of BU–TU diffusion functions are typically based on idealized LES model results (e.g., Moeng and Sullivan 1994; Patton et al. 2005; Vinuesa and Vila-Guerau de Arellano 2003). In this manuscript the correction for the mean tracer inversion is assumed to be proportional to Da [Eq. (10)]. The isoprene concentration gradient dc/dz in the mixed layer was 2.4×10^{-4} and 2.8×10^{-4} ppbv m^{-1} for RF6 and RF7, respectively. Based on the measured flux divergence we calculate a theoretical concentration gradient of 1.4×10^{-4} and 1.75×10^{-4} ppbv m^{-1}—thus, 37% and 41% lower than measured. After correction for the effect of chemical reactivity, the difference between modeled to measured dc/dz improves to 18% higher and 8% lower for RF6 and RF7, respectively. As a conservative limit, isoprene fluxes in the Amazon basin obtained by MLG method (Karl et al. 2007) have previously been corrected by about 14%. Taking estimated OH densities of 1.2–5 $\times$ 10^6 molecules per cubic centimeter and w^* of 2 m s^{-1}, Da was on the order of 0.08–0.19 during the Tropical Forest and Fire Emissions Experiment (TROFFEE) in the Amazon (Karl et al. 2007). Based on measurements presented here, we conclude that a simple first-order correction based on Da [Eq. (11)] can be used to correct isoprene fluxes obtained by the MLG method reasonably well.

5. Conclusions

We present novel eddy covariance measurements of isoprene during the CABERNET experiment. Vertically resolved measurements suggest that first-order chemistry can describe the decrease of isoprene fluxes throughout the PBL under typical atmospheric conditions. Experimentally determined Damköhler numbers were in the range of 0.3–0.9. Concentration gradients throughout the PBL are modified as a result of chemical reactions leading to locally smaller diffusion coefficients. Modification of turbulent diffusion coefficients have been proposed according to theoretical considerations developed for the surface layer (Kristensen et al. 1997). This improves the measurement-to-model comparison for a first-order nonlocal diffusion scheme. It is demonstrated that measurements of isoprene flux divergence can be used to study entrainment processes over land. Typical entrainment velocities observed during three research missions were 5.5, 9.6, and 1.4 cm s^{-1}, respectively. We propose that future airborne eddy covariance measurements of biogenic volatile organic compounds can be used to characterize heterogeneous surface emissions using wavelet decomposition and help develop a more robust land cover representation of reactive trace-gas fluxes. In addition, we demonstrate that flux divergence

measurements can be used to provide estimates of OH in the planetary boundary layer. Theses flux measurements can therefore provide a new way to determine average OH densities, allowing for investigation of potential OH recycling mechanisms that have been proposed to occur during isoprene oxidation.

Acknowledgments. This project was funded by the California Air Resources Board under Contract Number 09-339 to the University of California, Berkeley. We thank Roy Woods at CIRPAS for excellent mission support and the mission pilots Marko Jaakkola and Bryce Kujatat from ZIVKO Aeronautics for their dedicated help in flight preparation, planning, and execution. We thank Robin Weber and Abhinav Guha at the University of California, Berkeley, for logistical support.

APPENDIX A

Derivation of the Flux Detection Limit

The ensemble variance of a flux (i.e., covariance between w and c), where the integral time scale is much smaller than the averaging interval, is given by

$$\langle\sigma\rangle^2 = 4\sigma_c^2\sigma_w^2\frac{\Gamma_F}{T}, \tag{A1}$$

where σ_c (σ_w) is the standard deviation of the concentration c (vertical wind w) fluctuation, T is the averaging interval, and Γ_F represents the integral time scale of the flux. The error variance of a vertical flux due to counting noise (assuming a Gaussian distribution) is

$$\delta\sigma^2 = \sigma_w^2\langle c\rangle\frac{dt}{T}, \tag{A2}$$

where dt is the sampling time, T is the averaging time, $\langle c\rangle$ is the mean concentration, and σ_w is the standard deviation of the vertical wind.

The ratio between Eqs. (A1) and (A2) is $\langle c\rangle dt/4\sigma_c^2\Gamma_F$. This should be smaller than 1, so that we obtain

$$\frac{\langle c\rangle^2}{4\sigma_c^2} < \left\{\frac{\langle c\rangle\Gamma_F}{dt}\right\} := Q. \tag{A3}$$

We can introduce the instrument sensitivity as $S = Q/(\langle c\rangle\Gamma/dt)$. Based on observational data in the mixed layer, Lenschow and Kristensen (1985), for example, report that

$$\sigma_c \approx \frac{1.3F}{w^*}. \tag{A4}$$

Defining an exchange velocity ($v_e = F/\langle c\rangle$) analogous to a deposition velocity and inserting into Eq. (A4) and then into Eq. (A3), we obtain

$$Q > 0.15\frac{w^{*2}}{v_e^2}. \tag{A5}$$

APPENDIX B

Random and Systematic Errors due to Disjunct Sampling

For a more detailed derivation we refer to Lenschow et al. (1994).

The systematic error of the flux F due to disjunct sampling F_{disjunct} is given by

$$\frac{F - F_{\text{disjunct}}}{F} = \frac{\Delta}{\Gamma}\left\{\coth\left(\frac{\Delta}{2\Gamma}\right) - \frac{(\Delta/T)[1-\exp(-T/\Gamma)]}{2\sinh^2(\Delta/2\Gamma)}\right\}, \tag{B1}$$

where F represents the "true" (i.e., continuously sampled) flux.

For $T \gg \Gamma$, Eq. (B1) reduces to

$$\frac{F - F_{\text{disjunct}}}{F} = \begin{cases} 2\dfrac{\Gamma}{T} & \Delta \ll \Gamma \\ \dfrac{\Delta}{\Gamma} & \Delta \gg \Gamma \end{cases}. \tag{B2}$$

The relative random error variance due to disjunct sampling is described by

$$\frac{\sigma_{\text{disjunct}}^2}{\sigma^2} = \frac{\Delta}{2\Gamma}\coth\left(\frac{\Delta}{2\Gamma}\right). \tag{B3}$$

For $\Delta \ll \Gamma$ and $\Delta \gg \Gamma$, Eq. (B3) asymptotically reduces to

$$\frac{\sigma_{\text{disjunct}}}{\sigma} = \begin{cases} 1 & \Delta \ll \Gamma \\ \sqrt{2\dfrac{\Delta}{\Gamma}} & \Delta \gg \Gamma \end{cases}, \tag{B4}$$

where σ_{disjunct} is the standard deviation of the DEC flux and σ is the standard deviation of the true (i.e., continuously sampled) flux.

APPENDIX C

Steady-State Calculation for OH

In steady state, the OH (OH_{ss}) concentration is given by

$$\mathrm{OH} = \frac{P + R}{L}, \tag{C1}$$

where P represents the primary production

$$P = \frac{2j_{\mathrm{O}_3} k_1 [\mathrm{H_2O}][\mathrm{O_3}]}{k_2[\mathrm{M}]}, \tag{C2}$$

R represents the recycling efficiency, and L is the loss rate (e.g., determined by the OH reactivity).

In Eq. (C2), j_{O_3} represents the photolysis rate of O_3, k_1 is the rate coefficient between $O(^1D)$ and H_2O, and k_2 is the rate coefficient between $O(^1D)$ and M (i.e., air) leading to $O(^3P)$.

The recycling rate is approximated by the reaction of HO_2 with NO and O_3. NO is calculated for steady state as a function of NO_2:

$$\frac{\mathrm{NO_2}}{\mathrm{NO}} = \frac{k_3 \mathrm{O_3}}{j_{\mathrm{NO_2}}}, \tag{C3}$$

where k_3 is the reaction rate coefficient for the NO + O_3 reaction and $j_{\mathrm{NO_2}}$ is the photolysis rate for NO_2. Photolysis rates were calculated based on the Tropospheric Ultraviolet and Visible Radiation Model (TUV) (http://cprm.acd.ucar.edu/Models/TUV/).

The total OH reactivity L is assumed to be dominated by isoprene. The range for OH reactivity is varied within typical range of 3–15 s^{-1}.

REFERENCES

de Gouw, J., C. Warneke, T. Karl, G. Eerdekens, C. van der Veen, and R. Fall, 2003: Sensitivity and specificity of atmospheric trace gas detection by proton-transfer-reaction mass spectrometry. *Int. J. Mass Spectrom.,* **223,** 365–382.

Desjardins, R. L., and Coauthors, 1997: Scaling up flux measurements for the boreal forest using aircraft-tower combinations. *J. Geophys. Res.,* **102** (D24), 29 125–29 133.

Faloona, I., and Coauthors, 2005: Observations of entrainment in eastern Pacific marine stratocumulus using three conserved scalar. *J. Atmos. Sci.,* **62,** 3268–3285.

Goldstein, A. H., and I. E. Galbally, 2007: Known and unexplored organic constituents in the Earth's atmosphere. *Environ. Sci. Technol.,* **4,** 1514–152.

Greenberg, J. P., A. Guenther, P. Zimmerman, W. Baugh, C. Geron, K. Davis, D. Helmig, and L. F. Klinge, 1999: Tethered balloon measurements of biogenic VOCs in the atmospheric boundary layer. *Atmos. Environ.,* **33,** 855–867.

Guenther, A., C. N. Hewitt, D. Erickson, and R. Fall, 1995: A global model of natural volatile organic compound emissions. *J. Geophys. Res.,* **100** (D5), 8873–8892.

——, J. Greenberg, P. Harley, D. Helmig, L. Klinger, L. Vierling, P. Zimmerman, and C. Geron, 1996: Leaf, branch, stand and landscape scale measurements of volatile organic compound fluxes from U.S. woodlands. *Tree Physiol.,* **16,** 17–24.

——, T. Karl, P. Harley, C. Wiedinmyer, P. I. Palmer, and C. Geron, 2006: Estimates of global terrestrial isoprene emissions using MEGAN (Model of Emissions of Gases and Aerosols from Nature). *Atmos. Chem. Phys.,* **6,** 3181–3210.

Hamba, A., 1993: Modified *K* model for chemically reactive species in the planetary boundary layer. *J. Geophys. Res.,* **98** (D3), 5173–5182.

Hofzumahaus, A., and Coauthors, 2009: Amplified trace gas removal in the troposphere. *Science,* **324,** 1702–1704, doi:10.1126/science.1164566.

Hong, S. Y., Y. Noh, J. Dudhia, S. Korea, and M. M. Division, 2006: A new vertical diffusion package with an explicit treatment of entrainment processes. *Mon. Wea. Rev.,* **134,** 2318–2341.

Karl, T., C. Spirig, P. Prevost, C. Stroud, J. Rinne, J. Greenberg, R. Fall, and A. Guenther, 2002: Virtual disjunct eddy covariance measurements of organic trace compound fluxes from a subalpine forest using proton transfer reaction mass spectrometry. *Atmos. Chem. Phys.,* **2,** 279–291.

——, A. Guenther, R. J. Yokelson, J. Greenberg, M. Potosnak, D. R. Blake, and P. Artaxo, 2007: The tropical forest and fire emissions experiment: Emission, chemistry, and transport of biogenic volatile organic compounds in the lower atmosphere over Amazonia. *J. Geophys. Res.,* **112,** D18302, doi:10.1029/2007JD008539.

——, E. Apel, A. Hodzic, D. Riemer, D. Blake, and C. Wiedinmyer, 2009: Emissions of volatile organic compounds inferred from airborne flux measurements over a megacity. *Atmos. Chem. Phys.,* **9,** 271–285.

Kim, A., and Coauthors, 2013: Evaluation of HO_x sources and cycling using measurement constrained model calculations in a MBO and monoterpene dominated ecosystem. *Atmos. Chem. Phys.,* **13,** 2031–2044.

Kristensen, L., C. E. Andersen, and H. E. Jørgensen, 1997: First-order chemistry in the surface-flux layer. *J. Atmos. Chem.,* **2,** 249–269.

Lelieveld, J., and Coauthors, 2008: Atmospheric oxidation capacity sustained by a tropical forest. *Nature,* **452,** 737–740, doi:10.1038/nature06870.

Lenschow, D. H., and L. Kristensen, 1985: Uncorrelated noise in turbulence measurements. *J. Atmos. Oceanic Technol.,* **2,** 68–81.

——, C. A. Cullian, R. B. Friese, and E. N. Brown, 1978: The status of air motion measurements on NCAR aircraft. *Proc. Fourth Symp. on Meteorological Observations and Instrumentation,* Denver, CO, Amer. Meteor. Soc., 433–438.

——, A. C. Delany, B. B. Stankov, and D. H. Stedman, 1980: Airborne measurements of the vertical flux of ozone in the boundary layer. *Bound.-Layer Meteor.,* **19,** 249–265.

——, J. Mann, and L. Kristensen, 1994: How long is long enough when measuring fluxes and other turbulence statistics. *J. Atmos. Oceanic Technol.,* **11,** 661–673.

Lin, Y. L., and I. C. Jao, 1995: A numerical study of flow circulations in the Central Valley of California and formation mechanisms of the Fresno eddy. *Mon. Wea. Rev.,* **123,** 3227–3239.

Liu, Y., X. San Liang, and R. H. Weisberg, 2007: Rectification of the bias in the wavelet power spectrum. *J. Atmos. Oceanic Technol.,* **24,** 2093–2102.

Mauder, M., R. L. Desjardins, and I. MacPherson, 2007: Scale analysis of airborne flux measurements over heterogeneous terrain in a boreal ecosystem. *J. Geophys. Res.,* **112,** D13112, doi:10.1029/2006JD008133.

Mauldin, R. L., III, and Coauthors, 2012: A new atmospherically relevant oxidant of sulphur dioxide. *Nature,* **488,** 193–196, doi:10.1038/nature11278.

Metzger, S., and Coauthors, 2012: Spatial resolution and regionalization of airborne flux measurements using environmental response functions. *Biogeosci. Discuss.,* **9,** 15 937–16 003.

Moeng, C.-H., and P. P. Sullivan, 1994: A comparison of shear and buoyant driven planetary boundary layer flows. *J. Atmos. Sci.,* **51,** 999–1022.

Patton, E. G., K. J. Davis, M. C. Barth, and P. P. Sullivan, 2000: Decaying scalars emitted by a forest canopy: A numerical study. *Bound.-Layer Meteor.,* **100,** 91–129.

——, P. P. Sullivan, and K. J. Davis, 2003: The influence of a forest canopy on top-down and bottom-up diffusion in the planetary boundary layer. *Quart. J. Roy. Meteor. Soc.,* **129,** 1415–1434, doi:10.1256/qj.01.175.

——, ——, and C. H. Moeng, 2005: The influence of idealized heterogeneity on wet and dry planetary boundary layers coupled to the land surface. *J. Atmos. Sci.,* **62,** 2078–2097.

Petersen, A. C., and A. M. Holtslag, 1999: A first-order closure for covariances and fluxes of reactive species in the convective boundary layer. *J. Appl. Meteor.,* **38,** 1758–1776.

Schumann, U., 1989: Large-eddy simulation of turbulent diffusion with chemical reactions in the convective boundary layer. *Atmos. Environ.,* **23,** 1713–1727, doi:10.1016/0004-6981(89)90056-5.

Shilling, J. E., and Coauthors, 2013: Enhanced SOA formation from mixed anthropogenic and biogenic emissions during the CARES campaign. *Atmos. Chem. Phys.,* **13,** 2091–2113.

Spirig, C., A. Guenther, J. P. Greenberg, P. Calanca, and V. Tarveinen, 2004: Tethered balloon measurements of biogenic volatile organic compounds at a Boreal forest site. *Atmos. Chem. Phys.,* **4,** 215–229.

Thomas, C., and T. Foken, 2005: Detection of long-term coherent exchange over spruce forest. *Theor. Appl. Climatol.,* **80,** 91–104.

Torrence, C., and G. P. Compo, 1998: A practical guide to wavelet analysis. *Bull. Amer. Meteor. Soc.,* **79,** 61–78.

Troen, I., and L. Mahrt, 1986: A simple model of the atmospheric boundary layer sensitivity to surface evaporation. *Bound.-Layer Meteor.,* **37,** 129–148.

Vilà-Guerau de Arellano, J., N. Patton, T. Karl, K. van den Dries, M. C. Barth, and J. J. Orlando, 2011: The role of boundary layer dynamics on the diurnal evolution of isoprene and the hydroxyl radical over tropical forests. *J. Geophys. Res.,* **116,** D07304, doi:10.1029/2010JD014857.

Vinuesa, J., and J. Vilà-Guerau de Arellano, 2003: Fluxes and (co-) variances of reacting scalars in the convective boundary layer. *Tellus,* **55B,** 935–949.

Weil, J. C., and T. W. Horst, 1992: Footprint estimates for atmospheric flux measurements in the convective boundary layer. *Precipitation Scavenging and Atmosphere-Surface Exchange,* S. E. Schwartz and W. G. N. Slinn, Eds., Vol. 2, Hemisphere Publishing, 717–728.

Williams, J., and Coauthors, 2011: The summertime Boreal forest field measurement intensive (HUMPPA-COPEC-2010): An overview of meteorological and chemical influences. *Atmos. Chem. Phys.,* **11,** 10 599–10 618.